Superconducting incommensurate host-guest phases in compressed elemental sulfur

Jack Whaley-Baldwin [1,*] Michael Hutcheon [1] and Chris J. Pickard [2,3]

[1] *TCM Group, Cavendish Laboratory, University of Cambridge, Cambridge CB3 0HE, United Kingdom*

[2] *Department of Materials Science and Metallurgy, University of Cambridge, 27 Charles Babbage Road, Cambridge CB3 0FS, United Kingdom*

[3] *Advanced Institute for Materials Research, Tohoku University, 2-1-1 Katahira, Aoba, Sendai 980-8577, Japan*

(Received 17 March 2021; revised 21 May 2021; accepted 2 June 2021; published 21 June 2021; corrected 22 July 2021)

We use density functional theory (DFT) and structure searching methods to show that the ground state of elemental sulfur is a barium-IVa type incommensurate host-guest (HG) phase between 386 and 679 GPa, becoming the first group-VI element predicted to possess such a structure. Within the HG phase, sulfur undergoes a series of transitions in which adjacent guest chains are not aligned but rather offset by different amounts, which can be described as a rearrangement of the stacking order of the chains. We show that these chain rearrangements are intimately coupled to modulations of the host and guest atoms, which prove crucial to stabilizing the HG structure. Unlike the high-pressure HG phases of other elements, sulfur does not exhibit interstitial charge localization, and instead features strongly localized "voids" that are depleted of electronic charge. Prior to adopting the HG structure, we predict that sulfur possesses an orthorhombic structure of $Fdd2$ symmetry. We calculate the superconducting critical temperatures of these newly discovered phases, and we show that T_c is expected to peak between 24.8 and 28.2 K at 271 GPa.

DOI: 10.1103/PhysRevB.103.214111

I. INTRODUCTION

Sulfur (S) is an element renowned for its structural diversity, possessing a considerable array of metastable allotropes at ambient pressure alone [1,2]. This complexity persists at high pressures, where sulfur adopts elaborate catenated spiral structures above 1.5 GPa [3] and an incommensurately modulated structure at 83 GPa [4,5], which is driven by a charge density wave (CDW) instability.

Self-hosting incommensurate host-guest (HG) structures, which comprise two distinct elemental sublattices embedded within one another in such a way that the ratio of their lattice lengths along a certain crystal axis is an irrational number, are well known within the literature [6–16]. The reasoning behind the stability of such host-guest phases is often explained through so-called Fermi surface effects, sometimes referred to as the Jones mechanism [17], in which lattice distortions introduce Fourier components into the potential that lower the energy of Fermi level states.

The physical properties of these elemental host-guest structures are of great interest and vary significantly between elements. Several examples are superconducting, and they often exhibit high critical temperatures due to favorable low-frequency *quasi*acoustic phonon modes [11], with a record T_c of 29 K among all elements (excluding hydrogen) being calcium in just such a phase (Ca-VII at 210 GPa [18–20]). Conversely, other realizations of elemental HG structures feature large pseudogaps in their electronic densities of states at the Fermi level, and they form poorly conducting electrides with significant amounts of electronic charge localized in interstitial regions [7,9].

X-ray diffraction studies on S up to 165 GPa [4,5] and 250 GPa [21,22] have determined that S transforms from the incommensurately modulated CDW phase into the trigonal β-Po structure of $R\bar{3}m$ symmetry at ∼150 GPa. Several first-principles structure searching investigations [23–25] have predicted that the $R\bar{3}m$ structure remains stable up to ∼500 GPa, where S then adopts a body-centered-cubic (bcc) structure.

The correct determination of the crystal structure of S at high pressures is of interest to experimentalists in order to identify its presence as a decomposition product in high-pressure hydrogen sulfide experiments on H_2S and H_3S and to resolve the resulting diffraction pattern [26,27]. Knowledge of the true ground state is also important from a structure searching standpoint, so that the enthalpy of candidate H_2S/H_3S structures can be measured against decomposition into H and S [28,29].

The high-pressure superconducting properties of pure S have long attracted attention, and at one time it held the highest experimentally verified T_c in an element [30]. Further, the fact that the incommensurately modulated phase of S is superconducting with such a high T_c is unusual, as the Fermi-level gaps opened up by CDW formation often work to suppress superconductivity [31]. In addition to H_2S and H_3S, sulfur is a key constituent of several other high-T_c compounds, including a recently claimed room-temperature superconductor [32].

In this work, we investigate the phase diagram of S up to 700 GPa, and we report that under sufficient compression, S adopts a superconducting incommensurate HG structure similar to that of barium in the IVa phase [6], in addition to a previously unreported orthorhombic phase. We show that the guest structure in S undergoes several changes with increasing pressure, and we link this to modulations of the host and guest atoms. We further study the electronic structure and charge

*jajw4@cam.ac.uk

density distribution of the HG phase, and we compare the latter to other high-pressure HG structures.

II. COMPUTATIONAL DETAILS

We used the *ab initio* Random Structure Searching (AIRSS) package [33,34] for our structure searching, with the plane-wave DFT code CASTEP [35] performing the underlying electronic structure calculations. We generated a sulfur pseudopotential specifically designed for high-pressure work using the OTFG code in CASTEP (see the Supplemental Material [36]). Due to small enthalpy differences in certain parts of the phase diagram, we used an 850 eV plane-wave cutoff and a **k**-point spacing of $2\pi \times 0.01$ Å^{-1}, sufficient for absolute enthalpy convergence to ± 0.2 meV. Relative enthalpies between structures were converged to an even tighter tolerance. Geometry optimizations were carried out using the L-BFGS algorithm, and structures were relaxed until the forces on each atom were 5×10^{-4} eV/Å^{-1} or smaller, and the residual stresses 1×10^{-2} GPa or smaller.

We performed structure searches at 300, 400, 500, and 750 GPa, using randomly generated structures containing between 1 and 15 atoms and possessing between 1 and 48 symmetry operations. We then performed searches at these same pressures with 16, 21, 24, and 32 atoms. Finally, we performed much smaller searches in perturbed supercells of our various host-guest approximants, which involved up to 288 atoms. In total, we considered around 7500 fully relaxed structures.

III. RESULTS AND DISCUSSION

A. Relative enthalpies

Figure 1 shows our phase diagram of S calculated using the PBE functional. In addition to PBE, Table I shows the (static-lattice) transition pressures according to the LDA and PBEsol; the order of phase transitions is unaffected by the choice of functional. Using PBE, we determine that at 266 GPa, S transitions from the $R\bar{3}m$ (β-Po) phase to a structure of $Fdd2$ symmetry with 16 (64) atoms in its primitive (conventional) cell, which visually resembles a strongly distorted version of the Ba-IVa HG phase.

This $Fdd2$ structure is detailed in Figs. 2 and 3. While it clearly resembles the Ba-IVa HG structure, it has the property of being self-similar when rotated 45° about an axis perpendicular to the pseudoguest chains. We use the term pseudoguest, as this property implies that there is no longer a unique chain axis, and therefore it cannot be equivalent to the "standard" Ba-IVa type HG structure (although, as we will show, S does eventually adopt the Ba-IVa HG structure at higher pressures). The equivalence through a 45° rotation means that there are two nonintersecting pseudoguest chains, running in different directions in offset planes, as detailed in Fig. 3. Each pseudoguest chain forms part of the host structure when looking down the other chain's axis (and vice versa), and thus it is no longer possible to decompose the structure into two distinct host and guest lattices [see Figs. 2(b) and 2(c)]. While the pseudoguest chains in the same layer are in alignment, those in the layer below are shifted by half of the intrachain atomic separation, thus giving the chains an AB ordering when viewed from the side.

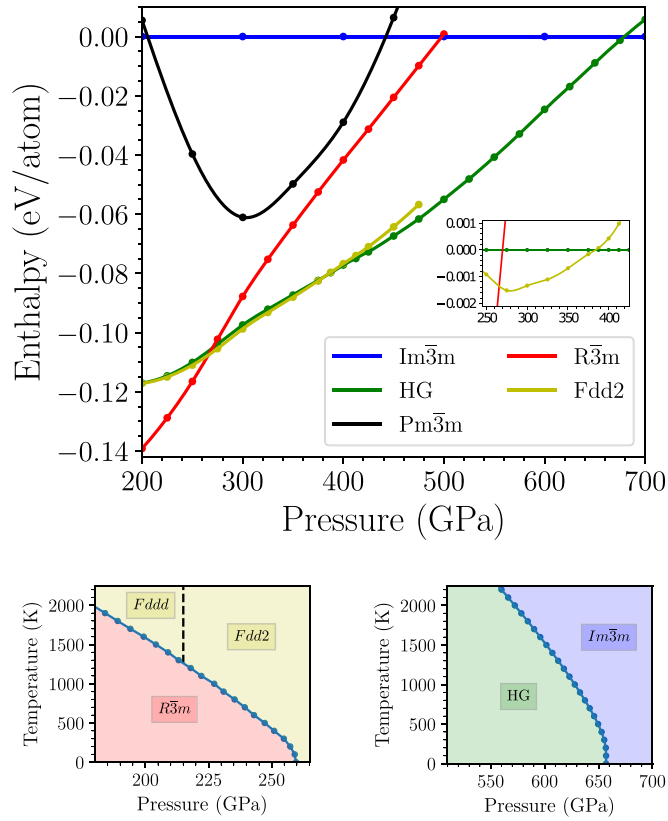

FIG. 1. Top: static-lattice phase diagram of S calculated with the PBE functional. "HG" denotes the host-guest phases, and for clarity, they have been plotted as a single curve. The inset shows the small enthalpy differences between the $Fdd2$ structure and HG phase. The simple-cubic $Pm\bar{3}m$ structure considered in previous studies [23–25,37,38] is shown for comparison. Bottom: phase diagrams with vibrational effects included (at the level of the harmonic approximation) in the vicinity of the $R\bar{3}m \rightarrow Fdd2$ transition (left) and HG $\rightarrow Im\bar{3}m$ transition (right). The black dashed line in the left diagram marks the boundary of the second-order $Fdd2 \rightarrow Fddd$ phase transition.

We tested the stability of this structure for a few other elements that possess a high-pressure HG phase (such as Al and As), but in each case it was never the lowest-enthalpy phase. The "two-chain" motif is reminiscent of the structure of the ternary incommensurate compound $Hg_{3-\delta}AsF_6$ [39–41], in which chains of mercury atoms, running at 90° to one another, sit within an AsF_6 framework. However, unlike this compound, and the incommensurate Ba-IVa phase,

TABLE I. Static-lattice transition pressures in GPa according to LDA, PBE, and PBEsol.

Functional	$R\bar{3}m \rightarrow Fdd2$	$Fdd2 \rightarrow$ HG	HG $\rightarrow Im\bar{3}m$
LDA	249	378	700
PBE	266	386	679
PBEsol	245	366	644

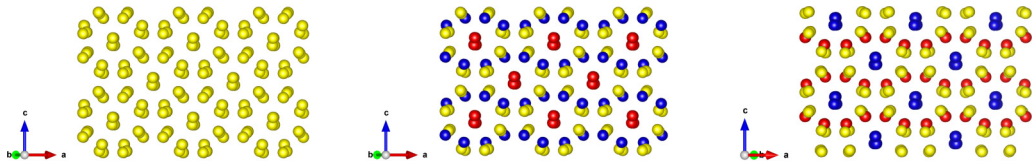

(a) (b) (c)

FIG. 2. The commensurate $Fdd2$ structure, viewed down the "pseudoguest" chains. The relation of this view to the lattice vectors of the conventional (64-atom) orthorhombic cell is shown in Fig. 3. (a) Looking down the pseudoguest chain axes. From top to bottom, the pseudoguest chains are arranged in an AB stacking. (b) The same structure, but with the two different types of pseudoguest chains artificially colored red and blue, shown looking down the axis of the red guests. (c) The same as the image on the immediate left, but rotated 45° clockwise around an axis running top to bottom of the page (i.e., perpendicular to the chains). The result is an equivalent structure.

our calculations suggest that the $Fdd2$ structure is in fact a commensurate crystal and is not *quasi*periodic. To demonstrate that this is the case, we first show that at higher pressures, S *does* exhibit a truly incommensurate Ba-IVa type HG structure, and then we use these findings to show that the $Fdd2$ phase cannot be incommensurate.

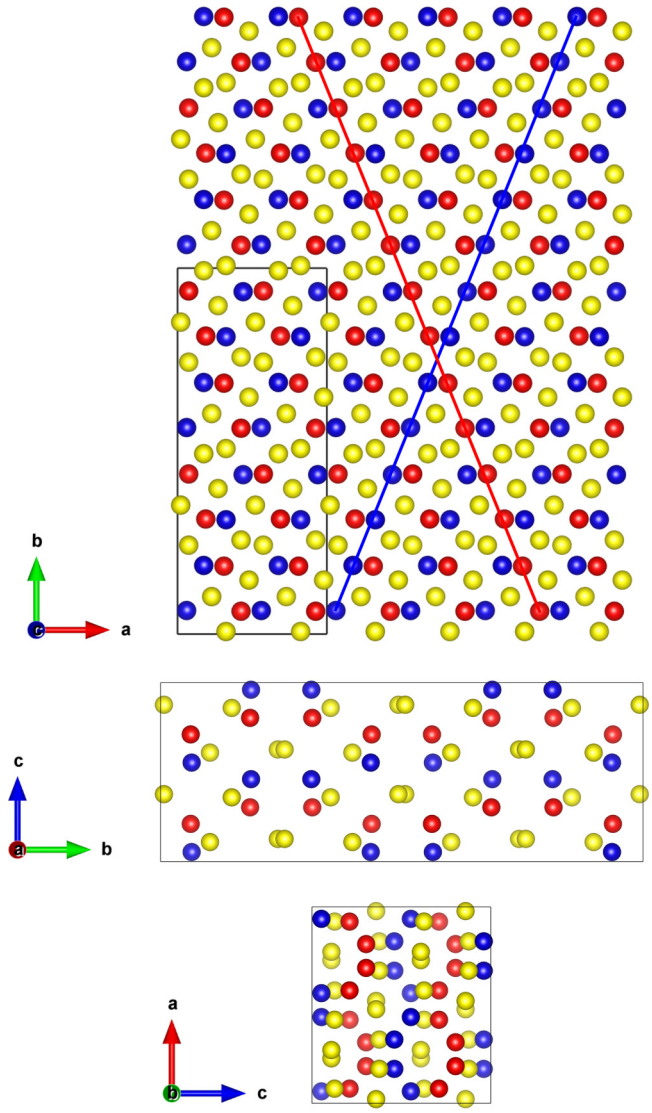

FIG. 3. The $Fdd2$ structure, in the same color scheme as Fig. 2. Two example chains (like those shown in Fig. 2) have been highlighted with red and blue lines (top figure only). The conventional (64-atom) orthorhombic unit cell is indicated in black.

The Ba-IVa HG structure, which occurs (with minor variations) in multiple elements across the Periodic Table [6–16], comprises a tetragonal "host" structure of $I4/mcm$ symmetry with eight atoms in the (conventional) unit cell, and one of two possible coexisting "guest" structures, either a C-face-centered-tetragonal structure, or an M-face-centered-monoclinic structure, with atoms at (0,0,0) and $(1/2, 1/2, 0)$ in both cases. The host and guest structures are incommensurate along their c-axes with an ideal ratio γ_0 that is remarkably close to $4/3$. In some cases, such as Bi-III and Sb-II [42,43] or Ca-VII [20], the positions of both the host and guest atoms in the HG structure are distorted/modulated relative to their "ideal" HG positions, giving both the channels and chains a "wiggly" or wormlike appearance.

We find that above 386 GPa, a Ba-IVa type HG approximant of $C2/c$ symmetry ($\gamma = 4/3$), with 16 (32) atoms in its primitive (conventional) cell, becomes lower in enthalpy than the $Fdd2$ structure. Similar to the $Fdd2$ structure, the atoms in the $C2/c$ approximant are distorted from their ideal positions; however, a unique chain axis for the guest atoms now exists, and thus the $C2/c$ approximant is of the "standard" Ba-IVa type. Below 386 GPa, the $C2/c$ approximant is dynamically unstable, and it develops an imaginary optical Γ-point phonon mode that leads to the $Fdd2$ structure. The structural and enthalpic differences between the $C2/c$ approximant and the $Fdd2$ structure are small, and over the stability range of the $Fdd2$, they differ in enthalpy by at most 1.5 meV per atom (see the inset in Fig. 1).

To calculate the ideal incommensurate host-guest ratio γ_0 at which the enthalpy is a minimum, we fitted the enthalpy of various commensurate approximants to a quadratic curve (see Supplemental Fig. 3 [36]), from which the ideal incommensurate ratio can be read off as the minimum. Figure 4 shows that γ_0 slowly decreases monotonically with increasing pressure, and that the choice of exchange-correlation functional does not affect the results significantly. This slow monotonic decrease in γ_0 with pressure is also seen in the HG phase of sodium [7], but is opposite to the cases of aluminum [9] and bismuth [43]. In potassium and rubidium, γ_0 initially decreases with pressure, before this behavior reverses and γ_0 instead increases with pressure [7].

The procedure used to calculate $\gamma_0(p)$ allows us to propose that the $Fdd2$ structure is *not* a commensurate approximant to an incommensurate phase, despite its visual similarity to the

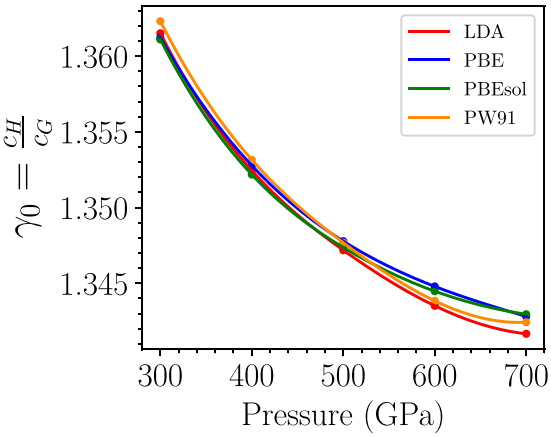

FIG. 4. Dependence of the ideal incommensurate ratio with pressure. Data were taken in 100 GPa intervals and fitted to a cubic spline.

Ba-IVa structure; of all the approximants used to construct our $H(\gamma)$ quadratic fits (9 in total), only the 16-atom approximant collapsed into the two-chain pattern at low pressures; approximants with other γ values simply remained in the "single chain" Ba-IVa type structure. This suggests that the $Fdd2$ structure does not belong to a family of HG approximants, but rather is a 16-atom structure in its own right. Additionally, we re-emphasize the fact that since one cannot decompose the $Fdd2$ into a unique host and a unique guest structure, it is not possible to even define a γ value for the $Fdd2$.

Relative to the more densely packed bcc ($Im\bar{3}m$) and trigonal ($R\bar{3}m$) phases, the HG structures are stabilized by a relatively large reduction in the total electronic energy. At 500 GPa, despite being ∼0.719% larger in volume, the HG phase has a total electronic energy 0.190 eV per atom lower than the bcc structure, which is more than enough to offset the increased pV term and make it a favorable structure. The idea that S becomes more open-packed at these pressures had previously been considered by Rudin *et al.* [37,38], who proposed an $R\bar{3}m \rightarrow$ simple-cubic ($Pm\bar{3}m$) transition, but neither that work nor two previous high-pressure structure searching studies [23,24] located the $Fdd2$ and HG phases. We further note the significance of our findings on the construction of convex hulls for sulfur compounds (e.g., H_2S and H_3S) at these pressures; the HG phase of S is lower in enthalpy than the previously assumed ground state ($R\bar{3}m$) by 11 meV per atom at 300 GPa, and up to 57 meV at 500 GPa.

The inclusion of nuclear vibrational effects does not change the phase transition sequence, and at low temperatures, vibrational zero-point energies (ZPEs) cause only small deviations from the static-lattice pressure boundaries (see Fig. 1). For example, at the $R\bar{3}m \rightarrow Fdd2$ transition, we find the ZPE of the $R\bar{3}m$ phase to be 1.4 meV per atom higher than that of the $Fdd2$ structure, which lowers the transition pressure by ∼4 GPa from the static-lattice value in Table I. The ZPEs of the $Fdd2$ structure and the $C2/c$ approximant are identical to within our convergence limits. At the HG → $Im\bar{3}m$ transition, we find the HG ZPE to be higher than that of the $Im\bar{3}m$ phase by 4.8 meV per atom, and the transition pressure reduces by ∼22 GPa compared to the value in Table I. At higher temperatures ($\gtrsim$300 K), vibrational effects reduce the transition pressures of both the $R\bar{3}m \rightarrow Fdd2$ and HG → $Im\bar{3}m$ transitions. The lowering of the transition pressure for the $R\bar{3}m \rightarrow Fdd2$ transition is particularly interesting for two reasons. First, it provides an experimental route to access the $Fdd2$ structure at slightly lower pressures, somewhat reducing the difficulty of any diamond anvil experiments. Second, it allows for observation of a new structure of $Fddd$ symmetry, also with 16 (64) atoms in its primitive (conventional) unit cell. This $Fddd$ structure is derived from the $Fdd2$ structure, which continuously develops an imaginary Γ-point phonon mode below 215 GPa, pushing it into the $Fddd$ symmetry—the resulting transition between the phases is thus second order. We note that this $Fddd$ structure is distinct from the well-known ambient-pressure orthorhombic ground state of sulfur (also of $Fddd$ symmetry) which comprises S8 rings. Our calculations show that at temperatures above ∼1260 K, the $Fddd$ phase should become the ground state at 215 GPa (again, see Fig. 1). We note that a recent publication [44] on the high-pressure melting curve of S achieved temperatures of ∼1700 K at 51 GPa using a laser-heated diamond anvil cell (LHDAC), and extrapolation of their data using a Simons-Glatzel fit [45] suggests that the melting temperature of S should be at least ∼3850 K at 200 GPa.

B. Chain ordering

After establishing the $Fdd2$ structure and $C2/c$ approximant as competitive phases, we conducted auxiliary searches with perturbed supercells of the $C2/c$ approximant containing 32, 64, 128, and 288 atoms. These searches produced two new HG approximants of $P4/ncc$ symmetry (32 atoms) and $Pcca$ symmetry (64 atoms) with slightly lower enthalpies. These approximants have the same commensurate ratio as the $C2/c$ approximant ($\gamma = 4/3$) and feature the same host structure, but they possess different guest structures. The bottom of Fig. 5 shows the relative enthalpies of these different host-guest approximants. It can be seen that the 16-atom $C2/c$ approximant is actually favored only in a narrow pressure range (384–400 GPa), before the 64-atom $Pcca$ approximant becomes favorable between 400 and 590 GPa. The 32-atom $P4/ncc$ approximant is then the ground state between 590 and 679 GPa, with the bcc $Im\bar{3}m$ phase becoming stable thereafter.

Each of the $C2/c$, $Pcca$, and $P4/ncc$ approximants represents a different ordering of the guest-atom chains, in which adjacent chains are displaced by a different amount parallel to the direction of the chain axes (i.e., have different heights in the z direction). We found that this displacement was always either 1/3 or 2/3 of the guest lattice c axis length (c_G). Figure 5 shows the different orderings as viewed along, and perpendicular to, the axes of the chains. In each case, the chains can clearly be described as having been stacked in a certain order, with the $C2/c$, $Pcca$, and $P4/ncc$ approximants possessing a stacking order of ABC, ABAC, and AB, respectively. Figure 5 also shows that the aforementioned distortions/modulations of the host and guest structures are slightly different in each case, being largest for the $C2/c$ structure and smallest for the $P4/ncc$ structure. This suggests a coupling between the chain orderings and the distortions, an observation that we shall return to later.

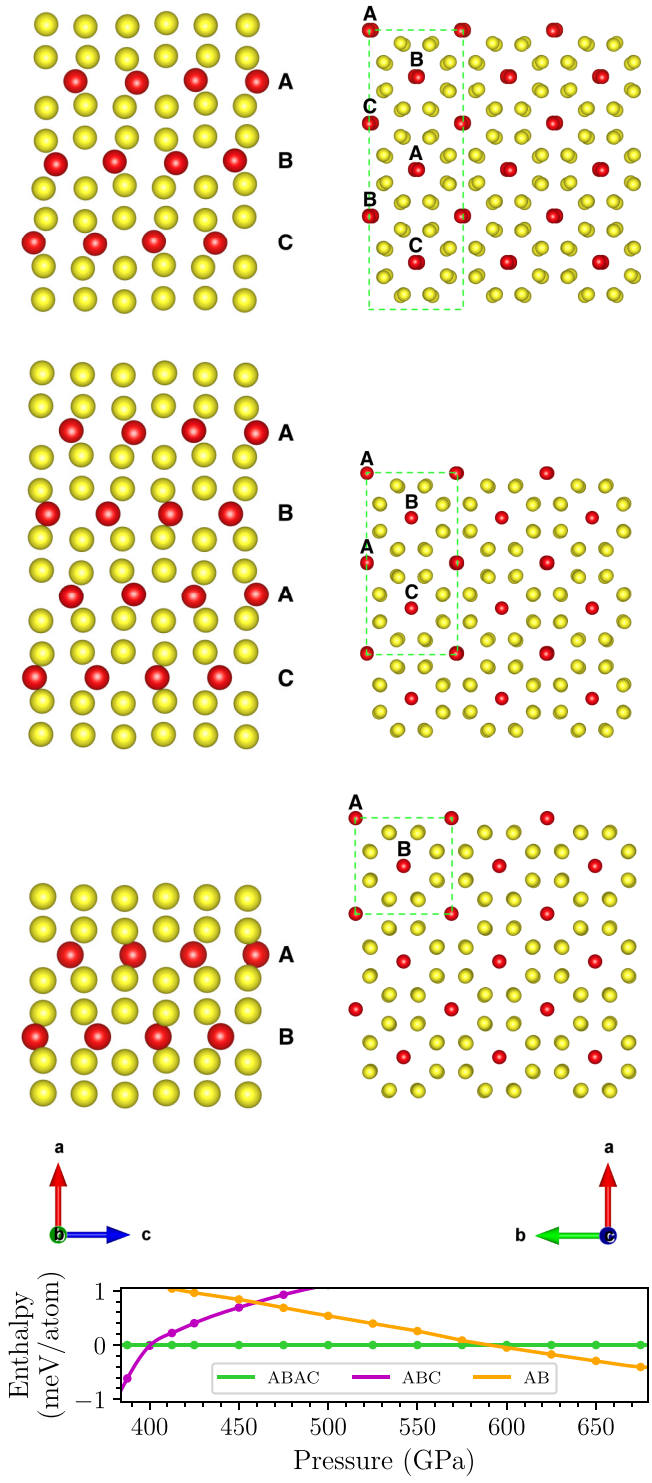

FIG. 5. Top: ABC $(0, \frac{1}{3}, \frac{2}{3})$ stacking of the 16-atom $C2/c$ approximant. Middle: ABAC $(0, \frac{1}{3}, 0, \frac{2}{3})$ stacking of the 64-atom $Pcca$ approximant. Bottom: AB $(0, \frac{2}{3})$ stacking of the 32-atom $P4/ncc$ approximant. The relative stability of the stackings is shown beneath the structures; the $Fdd2$ and bcc phases become stable immediately off to the left and right of the plot, respectively.

The lowest-enthalpy stacking ordering at a given pressure is a tradeoff between minimization of the total electronic energy and the pV term. The AB ordering of the $P4/ncc$ approximant stacks most efficiently to give the lowest pV term at all pressures, but it has the largest total electronic energy of all approximants. This situation is reversed in the ABC stacking of the $C2/c$ approximant, which has the lowest electronic energy but the largest pV term. The $Pcca$ approximant of ABAC stacking is a compromise between these two motifs and explains why it is favored over a comparatively large pressure range. At lower pressures (<400 GPa), the pV term is less important than the electronic term, and the $C2/c$ approximant becomes the ground state. At much larger pressures (>590 GPa), the pV term becomes dominant, and the $P4/ncc$ approximant is the lowest enthalpy phase.

Chain orderings that differ from the "ideal" all-aligned case have been discovered in other host-guest phases. The AB-ordered HG phase (our $P4/ncc$ approximant) that S adopts above 590 GPa is also the ground state of the group-V elements As, Sb, and Bi at much lower pressures [10,12]. The Ca-VII phase of calcium [20] is well-described by a 128-atom approximant in which the guest chains have different z-heights in both the a and b directions (as opposed to S, where the z-heights change only along the a direction). In the case of Ba-IVc, the structure adopted by barium at pressures a few GPa higher than the Ba-IVa phase, the chain displacements are arranged in such a way as to produce an extremely complicated, mesoscopic-scale, interlocking S-shape patterning, which is well-represented by a 768-atom cell [46].

While the enthalpy differences between the ABC, ABAC, and AB stackings are mostly ∼1 meV per atom, we note that the "ideal" stacking (of $I4/mcm$ symmetry), in which all guest chains are perfectly aligned (i.e., AAA…), is higher in enthalpy at all pressures by at least 20 meV per atom and up to 45 meV, indicating that perfect chain alignment is strongly disfavored in S. This raises the question of why any stacking that differs from the all-aligned case has such a drastically reduced enthalpy. Surprisingly, we find that explicitly offsetting the chains causes only a very small enthalpy reduction in itself. Instead, we show that the answer lies in the distortions/modulations of the host and guest atoms, which cannot occur unless the chains are first offset.

Figure 6 details the situation for the ABC case at 387 GPa, although the ABAC and AB cases are analogous. Starting from the all-aligned $I4/mcm$ approximant, we manually offset the chains so as to have an ABC ordering, keeping all else fixed. This gives rise to an enthalpy reduction of 4 meV per atom, which can be attributed to the opening of several directional band gaps at the Fermi level (see Supplemental Fig. 5 [36]). We subsequently relax the cell vectors (with the atomic positions fixed), which gives rise to a further enthalpy reduction of 1 meV. Finally, we add in the modulation of the host and guest atoms, which further reduces the enthalpy by 34 meV, an order of magnitude larger than the reductions caused by the chain offsets and the cell vector relaxation. The bottom of Fig. 6 shows that these energetic reductions arise as a result of shifting eDOS weight to lower energies, while little changes at the Fermi level itself.

Since the modulations provide the greatest contribution by far to the total enthalpy reduction, it is natural to ask why offsetting the guest chains—a change that causes only a very small enthalpy reduction in itself—is necessary to see these modulations appear. When the guest chains are offset, the host atoms are exposed to an asymmetric environment which

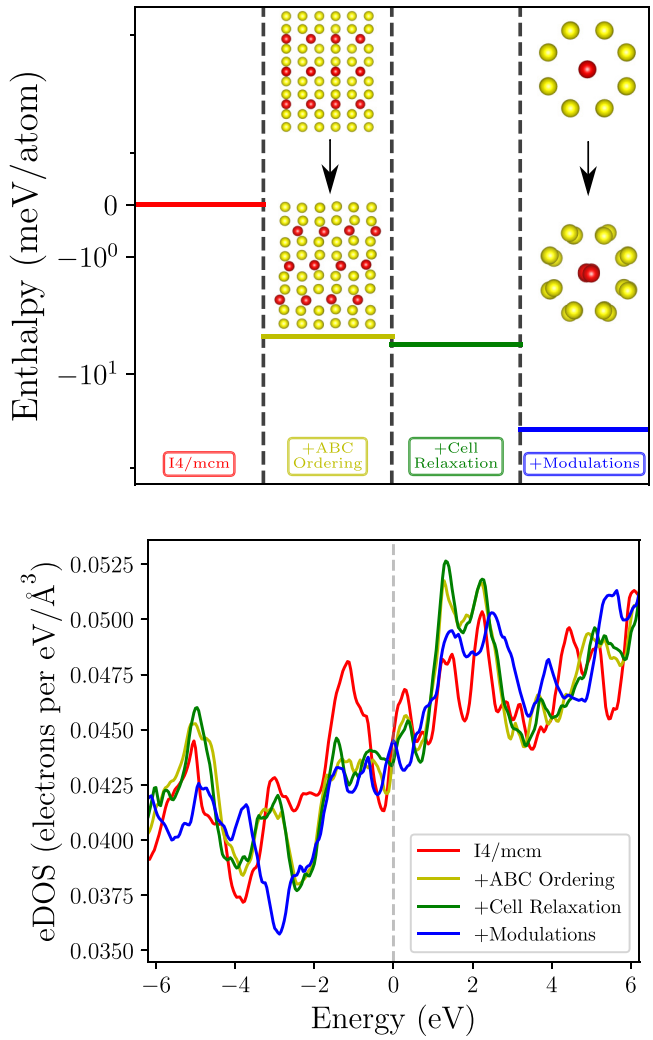

FIG. 6. Top: schematic decomposing the 39 meV enthalpy reduction that occurs going from the all-aligned approximant to the ABC ordered approximant at 387 GPa. The enthalpy axis is logarithmic. Bottom: the corresponding changes in the eDOS. The Fermi level is set at 0 eV.

creates forces that cause the host atoms to distort, which in turn distorts the guest atoms. If the chains are all-aligned, then the environment on either side of the host atoms is the same; symmetry implies that these forces do not arise, and there are therefore no distortions. In the ABC and ABAC stackings, both the host and guest atoms are distorted in all of the x, y, and z directions (see Fig. 5). However, in the case of AB stacking, symmetry dictates that the guests are displaced only in the z direction. These z distortions longitudinally pinch together pairs of guest atoms along the chain axes and dimerize them such that the covalent bonds alternate in a short-long-short-long pattern, with the short bond ∼3.2% smaller than the long bond. This 1D dimerization is referred to as *quasi*pairing in the literature [42], and the same behavior has recently been predicted to occur in the CDW phase of sulfur at lower pressures [24]. Detailed experimental [42] and theoretical [43] analyses of both the host and guest distortions in the Bi-III structure confirm that the modulations play an indispensable role in the stability of HG phases.

In addition to the structures found in our structure search, we calculated the enthalpy of various complex structures that appear in the vicinity of HG phases in other elements, such as oC52 in rubidium [47], oC84 in caesium [48], oP8 in potassium [49], and A7 in the group-V elements [12]. These structures were found to be at least 0.1 eV per atom above the ground state at all pressures considered here. We also constructed some $\gamma = 4/3$ approximants with longer-period chain stackings such as ABAAC, ABCAB, ABCACB, and permutations thereof, as well as configurations where the chain heights changed in the b-direction also (see the Supplemental Material for a table of all the stackings that were tested [36]). Most of these structures collapsed to the 64-atom *Pcca* ABAC stacking, which seems to have a particularly large basin of attraction in the configuration space of chain orderings. Those that did not collapse to the ABAC stacking simply had a higher enthalpy at all pressures, although we note that an ABCACB stacking was particularly close to becoming the ground state (+0.2 meV above the ABAC stacking at 550 GPa). We further considered the effect of spin polarization in our calculations, and seeded our structures with varying ferromagnetic and antiferromagnetic orderings, but in all cases the density relaxed to a spin-unpolarized configuration.

C. Charge density

We compare charge density isosurfaces of HG sulfur in Fig. 7 at moderate (35% of maximum) and very small (0.3% of maximum) values, alongside several 2D slices of the charge density taken perpendicular to the guest chains. The charge density of S is peaked near atomic sites and along lines connecting neighboring atoms, which is representative of a covalently bonded solid. S exhibits no significant interstitial localization of charge and therefore does not constitute a conventional electride, unlike the HG phases of the alkali metals [7] or aluminum [9]. However, S displays curious behavior when studied at very small isosurface values, which correspond to charge-depleted regions. The middle of Fig. 7 shows that these charge-depleted regions form well-localized lobes, which we refer to as charge "voids," and coincide with minima in the electron localization function (ELF) [50]. These voids form a structure equivalent to the host lattice of the alkali metal HG phases [7], with one host unit situated at the midpoint of every "short" intrachain covalent bond. The bottom of Fig. 7 shows the 2D charge density taken at the midpoints of these "short" bonds for the AB case; when these slices are superimposed, the full set of voids (as seen in the middle of Fig. 7) is recovered.

Remarkably, these voids are the exact locations of charge density *maxima* in the HG phase of aluminum [9]. The duality between the charge densities of S and Al can be explained in terms of the intrachain bonding between the guest atoms, which is present in S but absent in Al. In S, the short intrachain covalent bonds contain significantly more charge than the weaker long bonds; this excess charge is drawn from the charge voids, and explains why there is precisely one set of voids per short bond.

We note that in S there is no opening of a pseudogap in the electronic density of states (eDOS) at the Fermi level

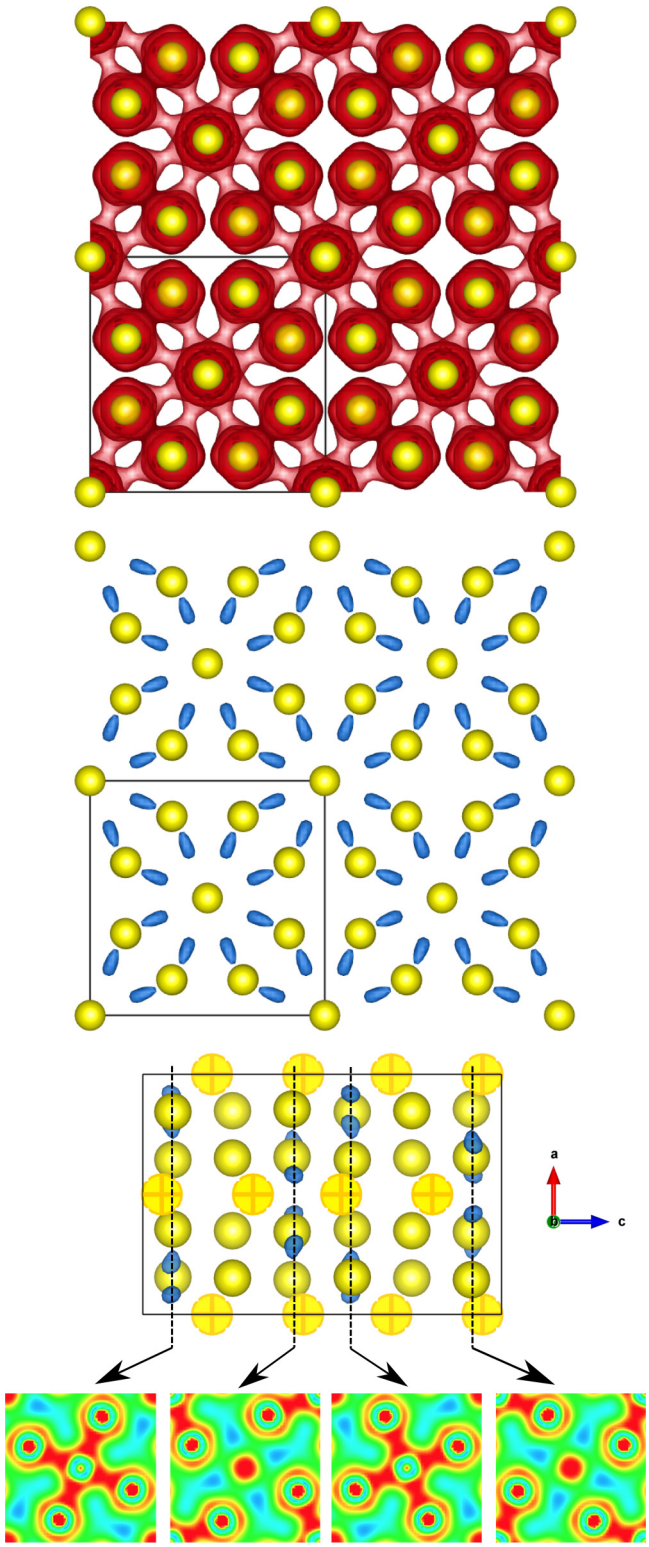

FIG. 7. Charge density in HG sulfur. Top: isosurface at 35% of maximum, displaying clear covalent bonds. Middle: isosurface at 0.3% of maximum, showing the charge-depleted "voids." Bottom: 2D slices of the charge density taken perpendicular to the guest chains for the AB ordering (guest atoms highlighted). The ABC and ABAC stackings give similar charge distributions, but the voids have different z coordinates in each case (as they are tied to the guest structure).

(see Fig. 6 and Supplemental Fig. 6 [36]). This is in contrast to the behavior of high-pressure electrides [7,9], in which there is often a dramatic reduction in the eDOS at the Fermi level (in Al, for example, the eDOS reduces by a factor of ∼4). Interestingly, we find that there is still significant $s \rightarrow d$ charge transfer in S; for the HG phase at 500 GPa, the Fermi-level eDOS comprises 11% s character, 42% p character, and 47% d character.

D. Superconductivity and phason modes

We have calculated the superconducting critical temperatures of our high-pressure sulfur phases using Migdal-Eliashberg theory within density functional perturbation theory (DFPT) using the QUANTUM ESPRESSO code [51]. We used the McMillan-Allen-Dynes formula [52] to calculate T_c:

$$T_c = \frac{\omega_{\log}}{1.2}\exp\left(\frac{-1.04(1+\lambda)}{\lambda - \mu^*(1+0.62\lambda)}\right), \tag{1}$$

where $\omega_{\log}$ is the logarithmically averaged phonon frequency, λ is the electron-phonon coupling constant, and μ^* is the Coulomb pseudopotential parameter, rescaled from the bare value μ to account for retardation [53]:

$$\mu^* = \frac{\mu}{1+\mu\ln\left(\frac{\epsilon_F}{\Theta_D}\right)}, \tag{2}$$

where ϵ_F is the Fermi energy and Θ_D is the phonon Debye frequency. We note that a relatively recent publication [54] has employed superconducting DFT (SCDFT) [55,56] to calculate the T_c of the $R\bar{3}m$ phase at pressures up to 200 GPa, and it shows that the value of μ for S in this regime remains nearly constant at 0.20. Rescaling this using Eq. (2), we obtain a μ^* value of 0.09 that is essentially constant across all the phases, since the ratio ϵ_F/Θ_D changes very little between the phases and with increasing pressure. Further, a previous publication [57] derived a μ^* value of 0.08 for the bcc phase at 500 GPa using the static Thomas-Fermi dielectric function. We therefore choose $\mu^* \in [0.08, 0.10]$ as a reasonable range of representative μ^* values.

Figure 8 shows our calculated T_c values as a function of pressure. It can be seen that T_c is expected to peak shortly after the transition to the $Fdd2$ phase, where we predict T_c to be 24.8–28.2 K at 271 GPa. For a purely elemental solid, this is a high critical temperature and is close to the record among the elements (excluding hydrogen) of 29 K in high-pressure Ca-VII [18–20]. Phonon calculations show that although it is not the lowest enthalpy phase at such pressures, the $Fdd2$ structure is dynamically stable down to pressures as low as 215 GPa (below here, it develops a soft mode that pushes it into the $Fddd$ structure, as previously mentioned). Since we find the T_c of the $Fdd2$ phase to be nearly constant in this region, it is possible that upon reducing pressure from >270 GPa, hysteresis effects may allow T_c to take a path similar to that indicated in purple in the top left of Fig. 8. We note that while T_c falls monotonically with pressure after the transition to the $Fdd2$ phase, we predict that S will remain superconducting up to at least 700 GPa.

While we used *isotropic* Migdal-Eliashberg theory to calculate T_c, we note that the aforementioned SCDFT calculations in Ref. [54] account fully for the Fermi surface

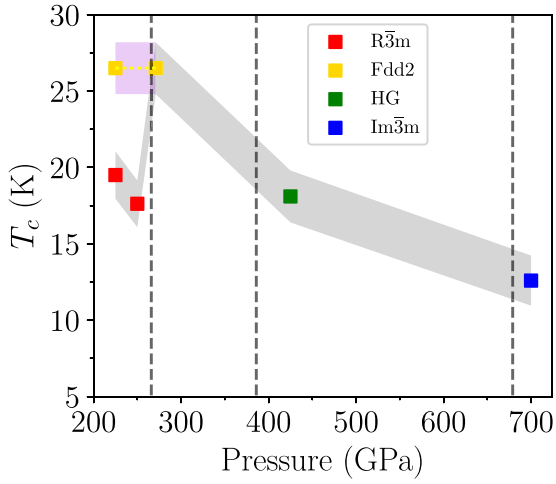

FIG. 8. Superconducting critical temperatures of the sulfur phases as a function of pressure. Dotted vertical lines denote the structural phase transitions discussed in this work. The shading corresponds to $\mu^* \in [0.08, 0.10]$; the gray region connects the lowest-enthalpy structures at each pressure, and the purple region in the top left is a possible metastable path if S can be trapped in the $Fdd2$ symmetry below 270 GPa. The data have been linearly interpolated.

anisotropy. Our T_c results for the $R\bar{3}m$ phase at 250 GPa are slightly higher (by ∼3 K) than the T_c obtained from the use of SCDFT in Ref. [54], although our Eliashberg function $\alpha^2F(\omega)$ is very similar (see Fig. 9). Conversely, our T_c value for the $R\bar{3}m$ structure is actually slightly lower (by ∼4 K) than the experimental value obtained by Drozdov *et al.* [22].

In the absence of complications such as the formation of finite-sized domains, the energy of a *truly incommensurate* HG structure must necessarily be invariant with respect to relative translation of the host and guest lattices. Such a relative translation can be achieved with an optical phonon mode running perpendicular to the guest chains, which displaces the host and guest structures in opposite directions. The energy of such a phonon mode should be exactly zero for a true *quasi*crystal, although the use of commensurate approximants in *ab initio* studies such as this work means that they appear to have a small positive frequency in a phonon calculation. Figure 10 shows the phonon dispersion relation for the AB-ordered $P4/ncc$ approximant, in which two low-energy optical modes can be seen. These "phason" modes naturally lead to large values of the mode-specific electron-phonon coupling constant $\lambda_{\mathbf{q},\nu}$, which varies with phonon frequency as $\sim\omega_{\mathbf{q},\nu}^{-1}$, and they give rise to strong-coupling superconductivity in HG phases [11]; however, as mentioned, our use of a commensurate approximant forces the phason modes in Fig. 10 to have a nonzero frequency. Consequently in Table II, which summarizes relevant superconducting properties of interest for several of the structures, the value of the electron-phonon coupling constant λ for the HG phase is *not* in the strong-coupling regime where $\lambda \gg 1$ [52]. It is probable that the use of a larger approximant (with accompanying lower phason frequencies) would give rise to a larger value of λ, although such a calculation is beyond the scope of this work and would be computationally expensive. We also note that solving the Eliashberg equations (necessary for the true strong-coupling case) gave very similar T_c values to those obtained using the McMillan-Allen-Dynes formula for all of the structures discussed in this work. Interestingly, we find that λ peaks in the $Fdd2$ phase, which by virtue

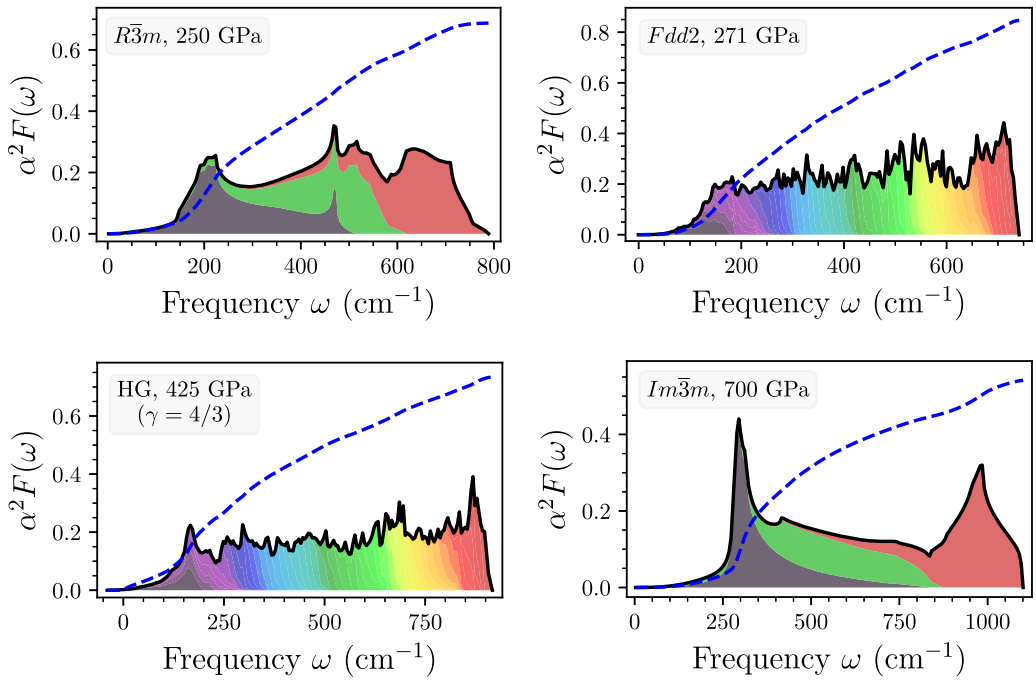

FIG. 9. Eliashberg function $\alpha^2F(\omega)$ for selected structures at given pressures. The contribution of each phonon branch to $\alpha^2F(\omega)$ has been shaded with a different color. The (cumulative) electron-phonon coupling constant $\lambda(\omega)$ has been plotted with a dashed blue line.

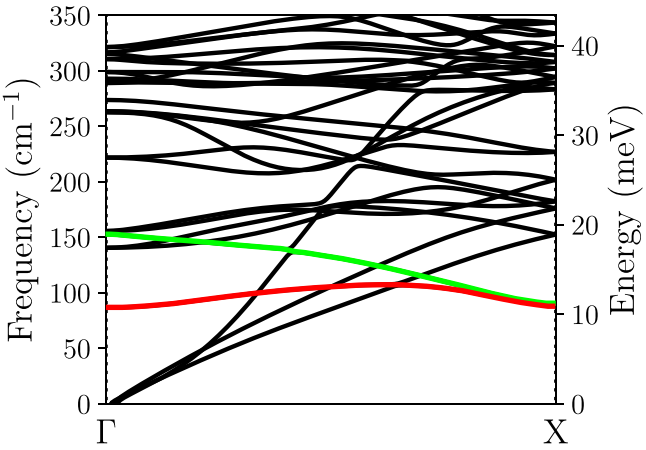

FIG. 10. Phonon dispersion relation for the AB-ordered $P4/ncc$ approximant at 375 GPa (commensurate ratio $\gamma = 4/3$). The $\Gamma \rightarrow X$ direction runs across the tetragonal face of the HG structure (perpendicular to the guest chains). Two low-energy phason modes, which correspond to relative movement of the host and guest lattices, have been highlighted in green and red. In the limit of a truly incommensurate structure, the frequencies of these modes vanish.

of being a commensurate structure cannot possess a phason mode. Nonetheless, we still predict a relatively high T_c of 16.4–19.8 K for the HG phase at 425 GPa, which we partially attribute to the lack of a significant Fermi-level pseudogap in the eDOS (see Table II).

IV. CONCLUSIONS

We have shown that upon increasing pressure beyond the experimentally known $R\bar{3}m$ (β-Po) phase, sulfur adopts a commensurate structure of $Fdd2$ symmetry in the range 266–386 GPa that resembles a strongly distorted Ba-IVa phase. Between 386 and 679 GPa, S possesses a truly incommensurate HG structure of the Ba-IVa type. Above 679 GPa, we find that S adopts a more closely packed bcc structure. We have accounted for the effects of finite temperatures on the phase boundaries, and we have shown that all of the transition pressures can be lowered with an increase in temperature, as well as predicting the existence of an $Fddd$ phase below 215 GPa and at temperatures $\gtrsim$1260 K.

TABLE II. Superconducting critical temperature T_c, electron-phonon coupling constant λ, logarithmic average frequency $\langle\omega_{\log}\rangle$, and Fermi-level electronic density of states $\mathcal{N}(\epsilon_F)$ (in units of electrons per eV per Å^3) for several of the structures discussed in this work at various pressures.

Structure	Pressure (GPa)	T_c (K)	λ	$\langle\omega_{\log}\rangle$ (K)	$\mathcal{N}(\epsilon_F)$
$R\bar{3}m$	250	17.6	0.689	469	0.0390
$Fdd2$	271	26.5	0.847	439	0.0414
HG ($\gamma = \frac{4}{3}$)	425	18.1	0.738	417	0.0445
$Im\bar{3}m$	700	12.6	0.543	660	0.0470

We have studied the properties of the incommensurate HG phase in detail, and we have shown that the ideal incommensurate ratio γ_0 decreases monotonically with increasing pressure. Over the stability range of the HG phase, S transforms between several competing chain-ordered variants of the incommensurate HG structure, with an ABAC chain stacking stable over most of this pressure range. These different chain orderings are intimately coupled to modulations of the host and guest atoms, which contribute substantially to the stability of the HG phases. We find that there is no significant interstitial localization of charge in S, instead showing that there are notable localized *absences* of charge ("voids"). We have calculated the superconducting critical temperature of S for several of the structures, and we expect T_c to peak between 24.8 and 28.2 K in the $Fdd2$ phase at 271 GPa. We predict that S remains a superconductor up to at least 700 GPa.

ACKNOWLEDGMENTS

We wish to thank Malte Grosche for useful discussions. The computational resources for this project were provided by the Cambridge Service for Data Driven Discovery (CSD3), and we are grateful for computational support from the UK national high performance computing service, ARCHER, for which access was obtained via the UKCP consortium and funded by EPSRC grant ref EP/K013564/1.

[1] B. Meyer, Chem. Rev. **64**, 429 (1964).
[2] B. Meyer, Chem. Rev. **76**, 367 (1976).
[3] O. Degtyareva, E. Gregoryanz, M. Somayazulu, P. Dera, H.-k. Mao, and R. J. Hemley, Nat. Mater. **4**, 152 (2005).
[4] O. Degtyareva, E. Gregoryanz, M. Somayazulu, H.-k. Mao, and R. J. Hemley, Phys. Rev. B **71**, 214104 (2005).
[5] H. Luo, R. G. Greene, and A. L. Ruoff, Phys. Rev. Lett. **71**, 2943 (1993).
[6] R. J. Nelmes, D. R. Allan, M. I. McMahon, and S. A. Belmonte, Phys. Rev. Lett. **83**, 4081 (1999).
[7] G. Woolman, V. Naden Robinson, M. Marqués, I. Loa, G. J. Ackland, and A. Hermann, Phys. Rev. Mater. **2**, 053604 (2018).
[8] U. Schwarz, A. Grzechnik, K. Syassen, I. Loa, and M. Hanfland, Phys. Rev. Lett. **83**, 4085 (1999).
[9] C. J. Pickard and R. J. Needs, Nat. Mater. **9**, 624 (2010).
[10] M. I. McMahon, O. Degtyareva, and R. J. Nelmes, Phys. Rev. Lett. **85**, 4896 (2000).
[11] P. Brown, K. Semeniuk, D. Wang, B. Monserrat, C. J. Pickard, and F. M. Grosche, Sci. Adv. **4**, eaao4793 (2018).
[12] U. Häussermann, K. Söderberg, and R. Norrestam, J. Am. Chem. Soc. **124**, 15359 (2002).
[13] M. I. McMahon, T. Bovornratanaraks, D. R. Allan, S. A. Belmonte, and R. J. Nelmes, Phys. Rev. B **61**, 3135 (2000).
[14] P. Tsuppayakorn-aek, W. Luo, W. Pungtrakoon, K. Chuenkingkeaw, T. Kaewmaraya, R. Ahuja, and T. Bovornratanaraks, J. Appl. Phys. **124**, 225901 (2018).
[15] O. Degtyareva, M. I. McMahon, and R. J. Nelmes, Phys. Rev. B **70**, 184119 (2004).
[16] S. Arapan, H.-k. Mao, and R. Ahuja, Proc. Natl. Acad. Sci. USA **105**, 20627 (2008).

[17] H. Jones and A. M. Tyndall, Proc. R. Soc. London, Ser. A **147**, 396 (1934).
[18] K. Shimizu, Phys. C **552**, 30 (2018).
[19] M. Sakata, Y. Nakamoto, K. Shimizu, T. Matsuoka, and Y. Ohishi, Phys. Rev. B **83**, 220512(R) (2011).
[20] H. Fujihisa, Y. Nakamoto, M. Sakata, K. Shimizu, T. Matsuoka, Y. Ohishi, H. Yamawaki, S. Takeya, and Y. Gotoh, Phys. Rev. Lett. **110**, 235501 (2013).
[21] E. Gregoryanz, V. V. Struzhkin, R. J. Hemley, M. I. Eremets, H.-k. Mao, and Y. A. Timofeev, Phys. Rev. B **65**, 064504 (2002).
[22] A. P. Drozdov, M. I. Eremets, I. A. Troyan, V. Ksenofontov, and S. I. Shylin, Nature **525**, 73 (2015).
[23] P. N. Gavryushkin, K. D. Litasov, S. S. Dobrosmislov, and Z. I. Popov, Phys. Status Solidi B **254**, 1600857 (2017).
[24] J. Whaley-Baldwin and R. Needs, New J. Phys. **22**, 023020 (2020).
[25] J. Whaley-Baldwin, Electron. Struct. **2**, 045003 (2020).
[26] A. F. Goncharov, S. S. Lobanov, I. Kruglov, X.-M. Zhao, X.-J. Chen, A. R. Oganov, Z. Konôpková, and V. B. Prakapenka, Phys. Rev. B **93**, 174105 (2016).
[27] D. Laniel, B. Winkler, E. Bykova, T. Fedotenko, S. Chariton, V. Milman, M. Bykov, V. Prakapenka, L. Dubrovinsky, and N. Dubrovinskaia, Phys. Rev. B **102**, 134109 (2020).
[28] T. T. Cui, D. Chen, J. C. Li, W. Gao, and Q. Jiang, New J. Phys. **21**, 033023 (2019).
[29] Y. Li, L. Wang, H. Liu, Y. Zhang, J. Hao, C. J. Pickard, J. R. Nelson, R. J. Needs, W. Li, Y. Huang, I. Errea, M. Calandra, F. Mauri, and Y. Ma, Phys. Rev. B **93**, 020103(R) (2016).
[30] V. V. Struzhkin, R. J. Hemley, H.-k. Mao, and Y. A. Timofeev, Nature **390**, 382 (1997).
[31] O. Degtyareva, M. V. Magnitskaya, J. Kohanoff, G. Profeta, S. Scandolo, M. Hanfland, M. I. McMahon, and E. Gregoryanz, Phys. Rev. Lett. **99**, 155505 (2007).
[32] E. Snider, N. Dasenbrock-Gammon, R. McBride, M. Debessai, H. Vindana, K. Vencatasamy, K. V. Lawler, A. Salamat, and R. P. Dias, Nature **586**, 373 (2020).
[33] C. J. Pickard and R. J. Needs, Phys. Rev. Lett. **97**, 045504 (2006).
[34] C. J. Pickard and R. J. Needs, J. Phys.: Condens. Matter **23**, 053201 (2011).
[35] S. J. Clark, M. D. Segall, C. J. Pickard, P. J. Hasnip, M. I. J. Probert, K. Refson, and M. C. Payne, Z. Krist. Cryst. Mater. **220**, 567 (2005).
[36] See Supplemental Material at http://link.aps.org/supplemental/10.1103/PhysRevB.103.214111 for pseudopotential information, convergence calculations, ideal host-guest ratio fitting procedure, enthalpy comparisons of other chain orderings, electronic band-structure plots, simulated diffraction patterns, comparisons of S to aluminum and arsenic, details of the superconducting critical temperature calculations, and structural information, which includes Refs. [58–68].
[37] S. P. Rudin and A. Y. Liu, Phys. Rev. Lett. **83**, 3049 (1999).
[38] S. P. Rudin, A. Y. Liu, J. K. Freericks, and A. Quandt, Phys. Rev. B **63**, 224107 (2001).
[39] J. D. Axe and P. Bak, Phys. Rev. B **26**, 4963 (1982).
[40] J. J. M. Buiting, M. Weger, and F. M. Mueller, J. Phys. F **14**, 2343 (1984).
[41] R. A. de Groot, J. J. M. Buiting, M. Weger, and F. M. Mueller, Phys. Rev. B **31**, 2881 (1985).
[42] M. I. McMahon, O. Degtyareva, R. J. Nelmes, S. van Smaalen, and L. Palatinus, Phys. Rev. B **75**, 184114 (2007).
[43] D. Kartoon and G. Makov, Phys. Rev. B **100**, 014104 (2019).
[44] S. M. Arveson, Y. Meng, J. Lee, and K. K. M. Lee, Phys. Rev. B **100**, 054106 (2019).
[45] F. Simon and G. Glatzel, Z. Anorg. Allg. Chem. **178**, 309 (1929).
[46] I. Loa, R. J. Nelmes, L. F. Lundegaard, and M. I. McMahon, Nat. Mater. **11**, 627 (2012).
[47] R. J. Nelmes, M. I. McMahon, J. S. Loveday, and S. Rekhi, Phys. Rev. Lett. **88**, 155503 (2002).
[48] M. I. McMahon, R. J. Nelmes, and S. Rekhi, Phys. Rev. Lett. **87**, 255502 (2001).
[49] L. F. Lundegaard, M. Marqués, G. Stinton, G. J. Ackland, R. J. Nelmes, and M. I. McMahon, Phys. Rev. B **80**, 020101(R) (2009).
[50] A. D. Becke and K. E. Edgecombe, J. Chem. Phys. **92**, 5397 (1990).
[51] P. Giannozzi *et al.*, J. Phys.: Condens. Matter **21**, 395502 (2009).
[52] P. B. Allen and R. C. Dynes, Phys. Rev. B **12**, 905 (1975).
[53] P. Morel and P. W. Anderson, Phys. Rev. **125**, 1263 (1962).
[54] M. Monni, F. Bernardini, A. Sanna, G. Profeta, and S. Massidda, Phys. Rev. B **95**, 064516 (2017).
[55] M. Lüders, M. A. L. Marques, N. N. Lathiotakis, A. Floris, G. Profeta, L. Fast, A. Continenza, S. Massidda, and E. K. U. Gross, Phys. Rev. B **72**, 024545 (2005).
[56] M. A. L. Marques, M. Lüders, N. N. Lathiotakis, G. Profeta, A. Floris, L. Fast, A. Continenza, E. K. U. Gross, and S. Massidda, Phys. Rev. B **72**, 024546 (2005).
[57] O. Zakharov and M. L. Cohen, Phys. Rev. B **52**, 12572 (1995).
[58] C. Hejny, L. F. Lundegaard, S. Falconi, M. I. McMahon, and M. Hanfland, Phys. Rev. B **71**, 020101(R) (2005).
[59] R. Jeanloz, P. M. Celliers, G. W. Collins, J. H. Eggert, K. K. M. Lee, R. S. McWilliams, S. Brygoo, and P. Loubeyre, Proc. Natl. Acad. Sci. USA **104**, 9172 (2007).
[60] J. Sun, M. Martinez-Canales, D. D. Klug, C. J. Pickard, and R. J. Needs, Phys. Rev. Lett. **108**, 045503 (2012).
[61] C. J. Pickard, M. Martinez-Canales, and R. J. Needs, Phys. Rev. Lett. **110**, 245701 (2013).
[62] P. Tsuppayakorn-aek, W. Luo, T. Watcharatharapong, R. Ahuja, and T. Bovornratanaraks, Sci. Rep. **8**, 5278 (2018).
[63] T. A. Strobel, P. Ganesh, M. Somayazulu, P. R. C. Kent, and R. J. Hemley, Phys. Rev. Lett. **107**, 255503 (2011).
[64] C. Liu, S. A. Nikolaev, W. Ren, and L. A. Burton, J. Mater. Chem. C **8**, 10551 (2020).
[65] C. J. Pickard, On-the-fly pseudopotential generation in CASTEP, University of St Andrews, United Kingdom (2006), http://www.tcm.phy.cam.ac.uk/castep/otfg.pdf.
[66] R. J. Nicholls, A. J. Morris, C. J Pickard, and J. R. Yates, J. Phys.: Conf. Ser. **371**, 012062 (2012).
[67] M. Wierzbowska, S. de Gironcoli, and P. Giannozzi, arXiv:cond-mat/0504077 [cond-mat.supr-con].
[68] M. L. Evans and A. J. Morris, J. Open Source Softw. **5**, 2563 (2020).

Correction: A second affiliation has been added for the third author.